International Journal of Civil and Structural Engineering Research ISSN 2348-7607 (Online)
Vol. 10, Issue 1, pp: (14-20), Month: April 2022 - September 2022, Available at: www.researchpublish.com

Damage Index Combination via Genetic Algorithm: A Highway Bridge Case Study

Elizabeth K. Ervin[1], Chuangshuo Zeng[2]

[1]University of Mississippi, University, MS, USA
[2]Sany Heavy Industry, Shanghai, China

Abstract: **Time histories often vary too much to determine root cause of signal shift. Frequency information and extracted modal properties can correlate to structural health through quantitative change metrics. Herein, fifty-one modal-based damage indices are considered in a total of three directions. These metrics are combined via vector resultants and Genetic Algorithm to visualize final relative stiffness results by location of data capture using a color code. This work presents inspection and data mining on an obsolete three-span truss highway bridge from 1953 or 1941 (disputed). Tri-axial deck data was captured in a grid for all three spans, and the new damage detection methodology is applied to Spans 1 and 2 with Span 3 as control. Comparative analysis among the three spans quantified joint effects, and end damages due to both scour and spalling were identifiable. Furthermore, unbiased analyses provided similar results to those biased by visual inspection. A more pointed visual inspection is thus permitted post-analysis.**

Keywords: **Modal Analysis, Data Mining, Genetic Algorithm, Bridge Inspection, Damage Detection.**

I. INTRODUCTION

This paper applies a new damage detection methodology to locate and quantify damage on a three-span highway bridge. In 2015 the MS Highway 7 Bridge over the Tallahatchie River was being replaced by a single-span prestressed concrete structure by the Mississippi Department of Transportation. The truss bridge was built in either 1953 or 1941 (disputed). Each simple span was "identical" at 120' long and 26' wide with 13'-6" vehicle and 20' overall truss height.

The Multi-Function Dynamics Laboratory in the Department of Civil Engineering at the University of Mississippi was given four hours to inspect said bridge before demolition. A quick cursory visual inspection noted (1) Span 1 had piers showing severe scour just above the water line, (2) Span 2 had a widely opened expansion joint at Span 1 showing spalling, and (3) overheight vehicle damage and both ends of the bridge. These items were confirmed by the lead supervisor; in fact, the new bridge opened days early due to his observation of concrete spalling in Span 2. Note that the actual condition of the deck underneath remains unknown.

The damage detection methodology compares two states of a structure, usually subsequent inspections of the same structure. Based upon observed bridge condition, Span 3 is considered the "control" in the numerical experiment. That is, Span 1 will be compared to Span 3 to quantify scour effects, and Span 2 will be compared to Span 3 to quantify expansion joint effects. This assumes that data can be affordably and conveniently captured by a bridge inspector; enough sensor time histories are taken to locate and quantify relative weakness; and frequency variations are due to damage rather than operating conditions. On the day of testing, the ambient temperature was steady near 30^{o}F, and the deck temperature ranged from 33.4^{o}F to 38.8^{o}F. Wind gusts of 15-20mph were predicted; the contractor measured a 13mph steady wind at one point.

The X, Y, and Z directions were selected to be the bridge's longitudinal, transverse, and vertical directions, respectively. Assumed level due to minimal road crowning, each span had 27 test locations: the deck grid was divided into nine points longitudinally at 15' spacing and three points laterally at 13' spacing. This results in a total of 81 nodes, but one point on Span 1 was omitted by accident. Each test node was sequentially measured under ambient vibration by a PCB Model 356B18 (1V/g) connected by traditional BNC cabling to a NI 9234 module in a NI CompactDAQ chassis, connected by USB to a laptop running NI LabVIEW (Figure 2). Accelerations were measured at 2048 Samples per second for 30 seconds. Examination of the time histories on Span 1 found a maximum longitudinal X-acceleration of 50.4±1.794mg, a maximum transverse Y-acceleration of 102.7±1.097mg, and a maximum vertical Z-acceleration of 35.8±1.247mg.

Frequency information was extracted from the 78 Span 1 traces (26 nodes x 3 directions), the 81 Span 2 traces (27 nodes x 3 directions), and Span 3 traces (both 78 and 81 trace sets). Fast-Fourier Transforms (FFTs) of the power 2^20 resulted in a frequency resolution of 0.001953Hz. The range of interest is 0.5 to 110Hz, and no filter or window was applied.

II. MODAL ANALYSIS

During modal decomposition, frequency peak selection is a crucial step, and peak-picking techniques vary widely. This step can be very time-consuming since the user has to sequentially check each frequency peak as well as the corresponding mode shapes. An open question is the order of operations for combining the 78 or 81 uni-directional FFTs into a single 3-D cumulative trace. To ease peak-picking and focus on stable peaks, eight combination methods are employed herein. Methods 1 through 3 provide similar results: all sum the directional channels and obtain magnitude, but Method 1 sums all directions, Method 2 takes the square root of the sum of the squares, and Method 3 takes the square root of the sum. Methods 4 and 5 provide similar results: Method 4 takes the magnitudes, sums all directions, and then sums all channels, while Method 5 normalizes the magnitudes before summing. Methods 6 through 8 provide similar results: all are based upon the power spectral density estimate via Welch's method with the full frequency range and 50% overlap. The resulting 78 or 81 smoothed traces are summed by all channels then directions (Methods 6 and 7) or summed by all directions then channels (Method 8). Method 6 simply sums all directions while Method 7 takes the square root of the sum.

After modal decomposition, matching modes is conducted by users and thus is subjective. Here, Modal Assurance Criterion (MAC) similarities and frequency differences are used to automate matching. Again, the open question of order of operations affects a 3-D resultant MAC. Uni-axial MAC is calculated as the square of the dot product of two mode shapes in one direction which is then normalized by both amplitudes [1]. Two forms of 3-D MAC are defined as “MAC R,” where each direction is summed and then a vector magnitude is taken, and “MAC S,” where the vector magnitude of the mode shape is taken before summing directions.

For matching of Spans 1 and 3, 26 test nodes and 78 captured signals were analyzed. Potential mode shapes considered include 54 Span 1 peaks and 61 Span 3 peaks for a possible combination of 3,294 matches. Fig. 1 shows the output plots of the 3-D MAC values. The yellow colors represent two potentially matching operational deflected shapes while dark blue shows dissimilarity. Any uni-directional MAC greater than 0.10 was considered of interest: this reduced the possible matches to 943. As the two spans are assumed “identical,” natural frequency variations should be relatively small; therefore, considering frequency differences of less than 2.5Hz further reduced possible matches to 91. These were examined by a human user, who found MAC R and MAC S could vary. An additional bin of the top 85% of both MAC R and MAC S proved useful. This provided 47 possible mode matches. Detailed examination of each possible match provided the five matched mode shapes in Table 1. All frequencies decreased in this case.

For matching of Spans 2 and 3, 27 test nodes and 81 captured signals were analyzed. Potential mode shapes considered include 31 Span 2 peaks and 64 Span 3 peaks for a possible combination of 1,984 matches. Any uni-directional MAC greater than 0.10 and frequency differences of less than 5Hz were considered of interest. The result was 282 possible mode matches. The additional bin of the top 95% of both MAC R and MAC S proved useful; this provided 47 possible mode matches. Detailed human examination of each possibility delivered the five matched mode shapes, also in Table 1. Note that Span 2 data provided a noisier FFT.

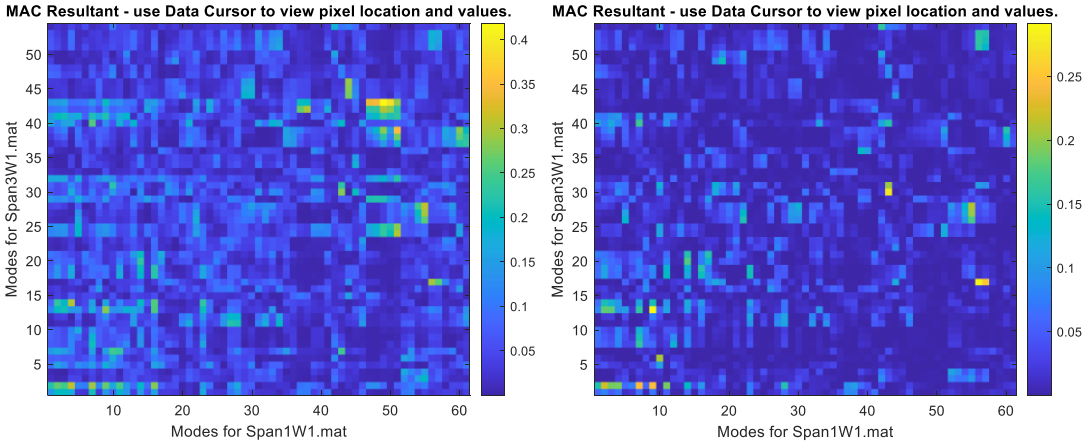

FIGURE 1: 3-D MAC R (left) AND MAC S (right) FOR 3,294 POSSIBLE MATCHES FOR SPAN 3 vs. 1.

III. DAMAGE DETECTION

A variety of quantitative metrics called Damage Indices (DI) have been proposed in literature. These involve some mathematical computation on a Damage Sensitive Feature (DSF) [2]. This work proposes that one single metric will not model all types of damage nor work for all types of structures. Rather, an artificially intelligent approach using the Genetic Algorithm (GA) can combine multiple metrics into the best model for each individual data set.

Yet again, the open question of order of operations affects a 3-D combination of each directional DI. The present study adopts two combination methods to calculate combined DIs generated from modal properties in three directions. Denoted Resultant or "R," the first method uses root sum square method to calculate a resultant DI using individual DIs in each x, y and z direction. A combined DI at the jth measured node is calculated as

$$DI_jR = \sqrt{{DI_{jx}}^2 + {DI_{jy}}^2 + {DI_{jz}}^2}$$

TABLE 1: MATCHED OPERATIONAL DEFLECTED SHAPES

Span 1 Freq. (Hz)	Span 3 Freq. (Hz)	MAC X	MAC Y	MAC Z	MAC R	MAC S	Freq. Difference (Hertz = Hz)
1.0918	2.5273	0.2508	0.1040	0.4593	0.3081	0.1922	-1.44
4.2598	4.4688	0.0337	0.1509	0.2443	0.1669	0.2062	-0.21
11.5371	11.7734	0.0509	0.0946	0.4300	0.2559	0.0966	-0.24
29.8984	30.7129	0.1953	0.0682	0.0631	0.1249	0.0572	-0.81
106.3301	108.3125	0.2744	0.0204	0.1076	0.1705	0.1569	-1.98
Span 2 Freq. (Hz)	**Span 3 Freq. (Hz)**	**MAC X**	**MAC Y**	**MAC Z**	**MAC R**	**MAC S**	**Freq. Difference (Hertz = Hz)**
1.3086	3.9805	0.0090	0.0847	0.1750	0.1124	0.0700	-2.67
4.2734	4.2852	0.0123	0.0384	0.1386	0.0833	0.1286	-0.01
7.1797	7.2070	0.0840	0.1428	0.4026	0.2514	0.3208	-0.03
13.9551	11.9531	0.0706	0.1288	0.0932	0.1004	0.0834	2.00
93.3164	93.3242	0.0822	0.4201	0.0895	0.2525	0.0708	-0.01

where DI_{jx}, DI_{jy}, and DI_{jz} are any DI calculated using only the modal properties in x, y and z directions, respectively. Denoted Spatial or "S," the second combination method first computes the magnitude of mode shapes before entering them into any single DI. The 3-D magnitude of a mode shape is calculated as

$$\varphi_iS = \sqrt{{\varphi_{ix}}^2 + {\varphi_{iy}}^2 + {\varphi_{iz}}^2}$$

where φ_{ix}, φ_{iy}, and φ_{iz} represent the mode shapes at ith measured node in x, y and z directions, respectively. In short, the first method takes a resultant of directional DIs, and the second method inserts a resultant mode shape into DI algorithm.

Herein, employed indices comprise four DSFs (mode shape deflection, flexibility [3], curvature [4] and [5], and strain energy [6]) calculated via common mathematical methods (difference [7], division [8], percentage [8], COMAC [9], probability [10], Z-score [10], and CDF [11]) where appropriate. Thus, 17 algorithms of uni-axial DIs are generated, and application in each of 3 directions produces 51 directional DIs. The Resultant and Spatial combination methods are then applied as appropriate to generate 24 combined three-dimensional DIs. Their nomenclature is (method)(DSF)(R or S).

The goal of implementing GA is to combine all 24 DIs into one single best-fit index. However, the magnitude of each DI can vary due to algorithm difference. To avoid numerical imbalance in combining DIs, each index is normalized so that their values are in the range of 0 to 1, showing percent possibility of damage. To also make the optimized DI indicate the possibility of damage, a weighted average function is built, and GA's objective function is minimizing the residual between this weighted average and a Target Vector (TV). An unbiased or unsupervised analysis would have identical weights in the TV, representing no *a priori* knowledge. A biased or supervised analysis has binary weights of both 0 and 1 in the TV, representing 0% or 100% suspected damage location from a visual inspection, for instance.

Based upon prior work, default settings on GA have been determined [12]. The solution tolerance is set to 1E-15, and the population size is 1,000. The maximum number of generations is set to 5,000, which was only met once in this work. The mutation function is adapt feasible with a ratio of 0.05. The crossover function is scattered with a fraction of 0.80. Three rounds of 5 runs each are employed in order to prevent missing a significant DI. A single DI is considered influential if its

weight function exceeds a threshold of 20%; any significant DIs are removed so as to analyze the remaining indices for their influence. A metric of success is the Fitness Value (FV): a lower FV indicates a better fit.

Using Span 3 as the control, GA was applied DIs for Spans 1 and 3 as well as Spans 2 and 3. The cases were analyzed: (1) unbiased with 100% TV, assuming damage everywhere; (2) unbiased with 0% TV, assuming no damage is expected; and (3) biased with 100% TV values where visual inspection indicated (scour or spalling), else 0% TV values. The most important output plot is the best fit indication of damage; for ease, a color code is employed. Damage is more likely with a higher possibility of damage percentage, so the bins are green (0-30%), blue (30%-50%), magenta (50%-70%), red (70%-90%), and black (90%-100%). Note that black indication does not mean a high percentage of collapse: it only quantifies a high possibility of relative structural weakness at the location. An inspector would be able to quickly focus in on potentially dangerous areas of the structure.

A. Results of Span 1 versus Span 3

Employing the same data and matched modes, Table 2 presents the GA results for all three cases of TV. Recall that Round 1 includes all 24 DIs while Rounds 2 and 3 examine reduced numbers of less influential DIs. Therefore, it makes sense that the Fitness Value (FV) increases with subsequent analyses, showing a lesser fit. Note that the unbiased damage detection results with 100% TV is unsuccessful. An inspector would not be able to decipher a relative weakness since indication varies between 15% to 36%, less than a 50% chance everywhere. The FVs are more than double any other TV case, indicating poorer fit. Round 1 uses a remarkable 12 of 24 DIs to attempt to make any kind of fit.

Fig. 2 (left) shows successful damage detection with a 0% TV: numerically significant detection of 86% is shown at one expected location without target bias. No false positives exist, but (x,y)=(0 feet, 0 feet) exhibits what appears to be a false negative. Perhaps the support scour was much more significant at (x,y)=(0 feet, 26 feet), so much so that it also affects (x,y)=(15 feet, 26 feet). However, this result is Round 2, not Round 1 in which an extreme outlier at (x,y)=(30 feet, 0 feet). Future work must examine if a noisy signal at one location is magnified by the normalization process, especially for low level TVs. Test node resolution also needs further examination.

Fig. 2 (right) also shows successful biased damage detection: numerically significant detection of 88% is shown at one expected location. No false positives exist, but (x,y)=(0 feet, 0 feet) exhibits a low 27% possibility of damage, which could be numerical or actual. Interpretation of a biased damage detection plot requires more attention to detection range as this study quantifies the relative weakness with bias for specific locations. Note that Table 4 shows that Round 2 with the biased TV did not converge, meeting maximum generations. Therefore, Rounds 2 and 3 should be omitted.

Here, the similarity between the unbiased and biased plots in Fig. 2 is extraordinary. The most indicated point (x,y)=(0 feet, 26 feet) measures 86% and 88% while the second most indicated point (x,y)=(15 feet, 26 feet) measures identically at 44%. This consistency would leave a user with more confidence regarding these results. The FV of the biased case versus the unbiased case is lower, indicating a better fit as expected. The number of generations to fit is nearly interchangeable, but the unbiased case took 777% longer to run. The unbiased case selected 100% Spatial Strain Energy Percentage (percSES) and 100% Spatial Strain Energy Division (divSES); the biased case also selected 64.35% percSES and 27.96% divSES along with 100% Z-normalized Strain Energy (ZSE). The unbiased and biased cases removed four and ten DIs, respectively, from the fit with percentages under 0.001%.

TABLE 2: DAMAGE DETECTION RESULTS FOR SPANS 1 VERSUS 3

Unbiased Target Vector = 100%

	Fitness Value (FV)	Generations to Stop (max 5000)	Number of DIs in Fit	Description of Damage Indication
Round 1, 5 Runs	2.2892	1948	12	None clear
Round 2, 5 Runs	2.6891	852	4	None clear
Round 3, 5 Runs	2.6210	411	3	None clear

Unbiased Target Vector = 0%

	Fitness Value (FV)	Generations to Stop (max 5000)	Number of DIs in Fit	Description of Damage Indication
Round 1, 5 Runs	1.0774	1397	3	Outlier Node at (30 ft, 0 ft)
Round 2, 5 Runs	1.1293	1198	2	Correct End Nodes
Round 3, 5 Runs	1.3450	1408	2	Correct End Nodes, more scatter

Biased Target Vector = 2 End Points

	Fitness Value (FV)	Generations to Stop (max 5000)	Number of DIs in Fit	Description of Damage Indication
Round 1, 5 Runs	0.9810	1121	3	Correct End Nodes
Round 2, 5 Runs	1.6147	5000	5	Correct End Nodes, more scatter
Round 3, 5 Runs	1.6745	941	3	Scatter

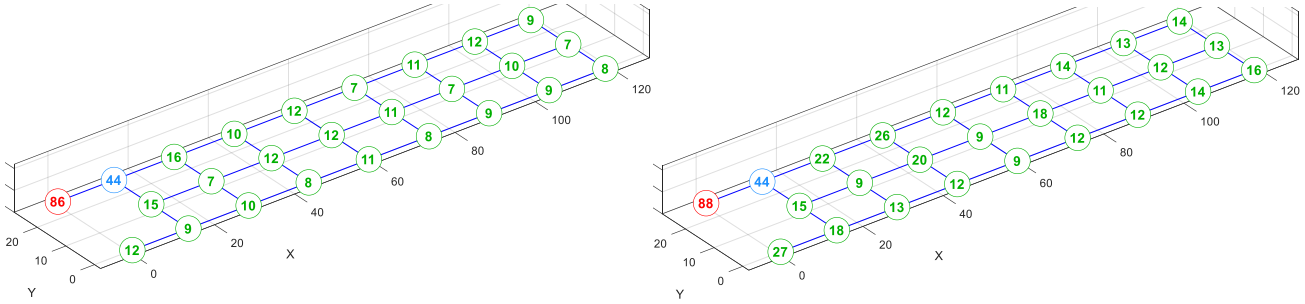

FIGURE 2: DAMAGE DETECTION RESULTS FOR SPANS 1 VERSUS 3: (left) UNBIASED WITH 0% TV, (left) BIASED WITH VARIED TV

B. Results of Span 2 versus Span 3

Employing the same data and matched modes, Table 3 presents the GA results for all three cases of TV. Recall that Round 1 includes all 24 DIs while Rounds 2 and 3 examine reduced numbers of less influential DIs. Therefore, it makes sense that the Fitness Value (FV) increases with subsequent analyses, showing a lesser fit. The unbiased damage detection results with 100% TV is again unsuccessful. An inspector would not be able to decipher a relative weakness since indication varies between 18% to 39%, less than a 50% chance everywhere. The FVs are high, and Round 1 uses too many DIs to make any kind of fit.

TABLE 3: DAMAGE DETECTION RESULTS FOR SPANS 2 VERSUS 3

Unbiased Target Vector = 100%

	Fitness Value (FV)	Generations to Stop (max 5000)	Number of DIs in Fit	Description of Damage Indication
Round 1, 5 Runs	2.0015	1435	12	None Clear
Round 2, 5 Runs	3.0219	1388	6	None Clear
Round 3, 5 Runs	3.4026	316	2	None Clear

Unbiased Target Vector = 0%

	Fitness Value (FV)	Generations to Stop (max 5000)	Number of DIs in Fit	Description of Damage Indication
Round 1, 5 Runs	1.0121	1027	2	Correct end, single point
Round 2, 5 Runs	1.1098	952	1	Wrong location
Round 3, 5 Runs	1.2238	933	3	Correct end, multiple points

Biased Target Vector = 3 End Points

	Fitness Value (FV)	Generations to Stop (max 5000)	Number of DIs in Fit	Description of Damage Indication
Round 1, 5 Runs	1.7736	814	4	Correct end, wrong point, scatter
Round 2, 5 Runs	1.9362	750	2	Correct end, wrong point
Round 3, 5 Runs	2.0896	696	6	Correct end, wrong point

Fig.3 illustrates the three rounds of best fit for the unbiased damage detection results using 0% TV. Fitness Values are reasonable (1.01-1.22) and increase with round number as expected. Using 2 of 24 DIs, Round 1 results in a single point of 98% detection at (x,y)=(30 feet, 26 feet); this is a possibility but not an expected point directly on the damaged expansion joint. However, the substructure's condition was unknown for Span 2. Using just 1 of 22 DIs, Round 2 produces an unexpected point (x,y)=(90 feet, 13 feet) with a 95% indication. One DI alone raises suspicion of an outlier, but this is possible. Using 3 of 21 DIs, Round 3 results in more likely points, 97% at (x,y)=(15 feet, 0 feet) and 59% at (x,y)=(15 feet, 15 feet) 59%. These are at the correct end, but again a bit further towards mid-span than expected.

Fig. 4 provides the three rounds of best fit for the biased damage detection results using fully damage indication at the three end points of x=0 feet. All rounds show damage at the correct end but not the expected end points on the expansion joint. Because the substructure's condition was unknown, perhaps the damage really was worse underneath point nearby the expansion joint. At 1.77-2.09, Fitness Values are surprisingly higher than the unbiased case (1.01-1.22); this may indicate a lower ability of the data fitting the expected damage.

Using 4 of 24 DIs, Round 1 shows some scatter with a maximum of 72% detection at (x,y)=(30 feet, 26 feet); this is the same point of the unbiased 0% TV but with a greater indication of 98%. Using 2 of 20 DIs, Round 2 produces a possible damaged point of (x,y)=(15 feet, 0 feet) with a 85% indication. Using 6 of 18 DIs, Round 3 results are similar to Round 2 but with a lower maximum at 55% at (x,y)=(15 feet, 0 feet).

IV. CONCLUSION

Prior studies as well as this work show that damage detection using 100% does not provide reasonable output [12]. For both comparisons to Span 3, the unbiased 0% TV produced the same or perhaps better results in both fit and detection than the biased TV with end point damage. This is an exciting outcome because it implies that an *a priori* visual inspection is not required for this bridge span comparison.

Prior studies showed that end damage is most identifiable because support conditions affect every mode shape [13]. Herein, Fig. 2 would send an inspector to the correct end of Span 1 where scour exists. The data mining is consistent with the visual inspection. Five of the six illustrations in Figs. 3 and 4 would also send an inspector to the correct quarter of Span 2 where spalling has occurred. The visual inspection notes end damage, but the data mining shows more structural damage within 30 feet of the concerning expansion joint. Still, a more pointed visual inspection is permitted post-analysis.

Round 1 should always be carefully considered as it uses all 24 3-D Damage Indices. A round with an outlier result is difficult to recognize, but use of any GA stopping criterion besides tolerance is a clear identifier. Other considerations include use of a single fit DI and an inconsistent location to other rounds. Additionally, too much scatter often involves a poor detection range and large numbers of DIs attempting a fit.

This work is based upon several hypotheses that may introduce uncertainty. Considering Span 3 as a control implies that this span does not have damage of its own. End damage is assumed to be the physical effect; for instance, the expansion joint damage may have been superficial, and the contractor observed spalling was closer to mid-span from the substructure. Regarding the data capture, time and cost were deemed the limiting factor to number of test nodes and sensor connections. More points should always be better, but constraints will always need to be considered. Lastly, it is assumed that wind excitation was enough excitation to show damage through tri-axial coupling.

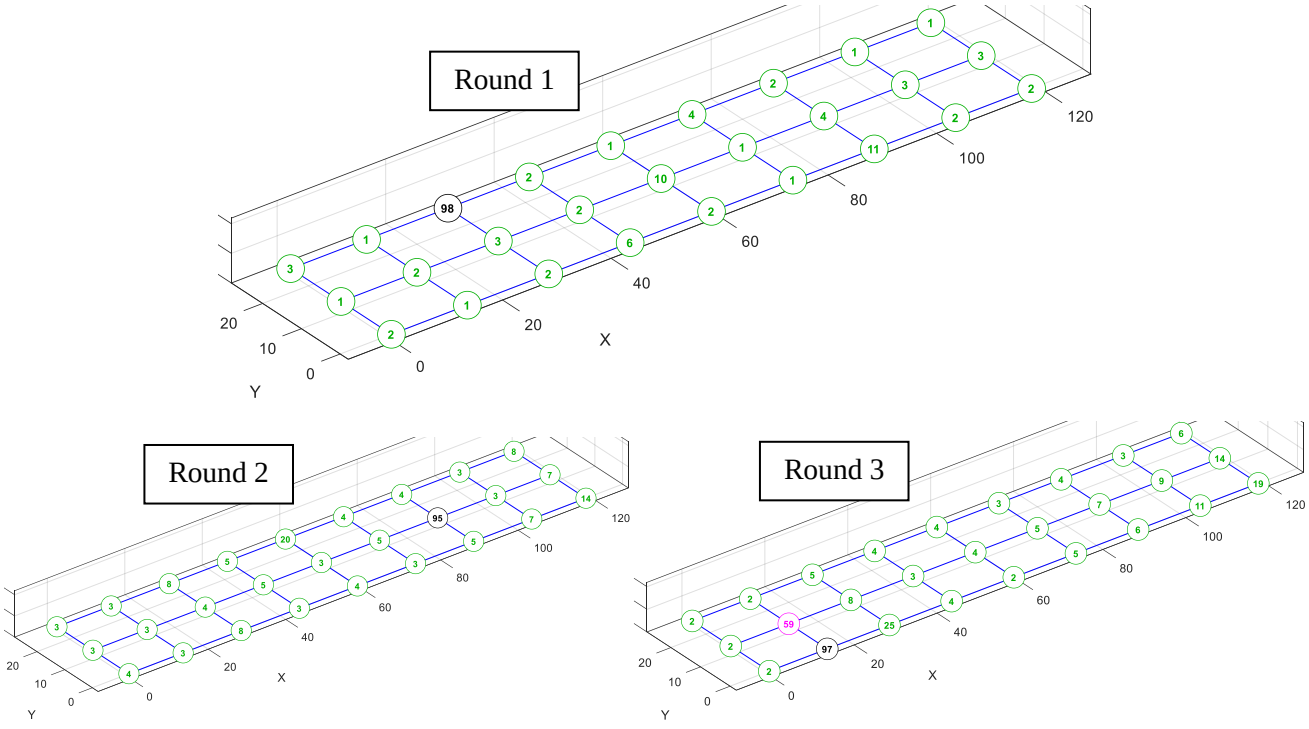

FIGURE 3: UNBIASED DAMAGE DETECTION RESULTS FOR SPANS 2 VERSUS 3

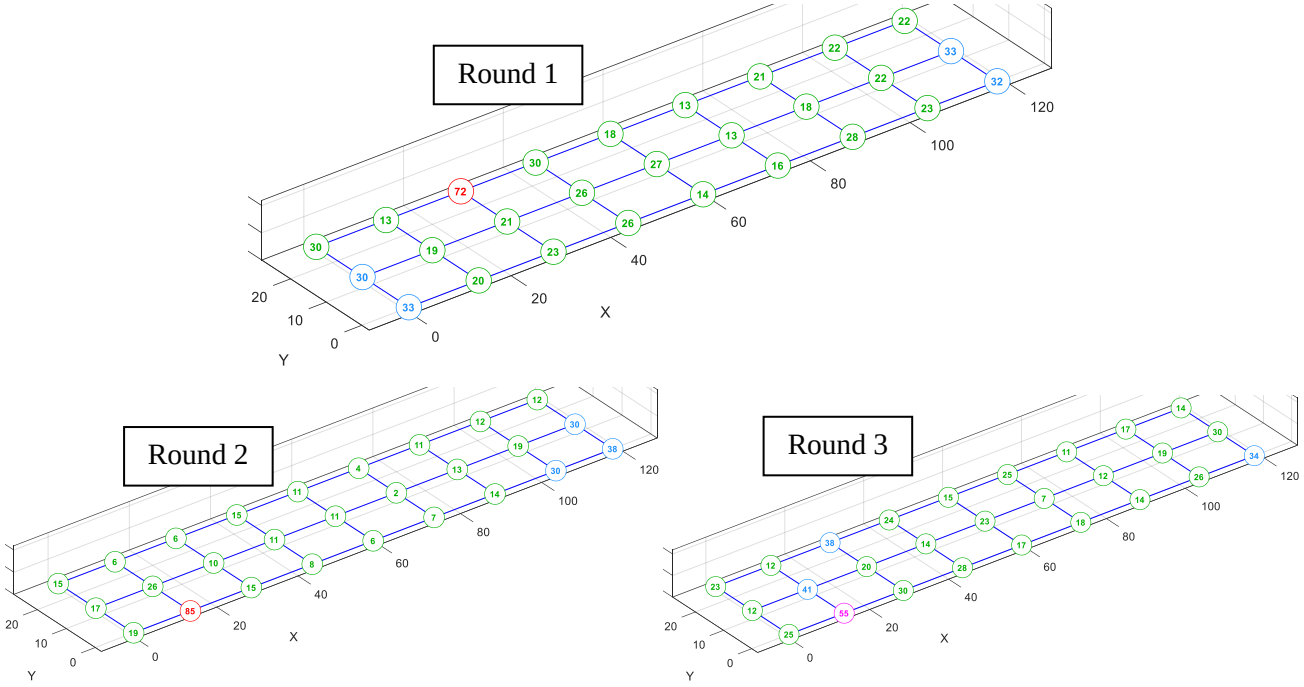

FIGURE 4: BIASED DAMAGE DETECTION RESULTS FOR SPANS 2 VERSUS 3

REFERENCES

[1] R. Allemang and D. Brown, "A Correlation Coefficient for Modal Vector Analysis," Proc. of the 1st International Modal Analysis Conference, Orlando, FL, 1982.

[2] R. Farrar and K. Worden, Structural Health Monitoring: A Machine Learning Perspective, 1st ed., Wiley, 2012.

[3] HN. P. Moragaspitiya, D. P. Thambiratnam, N. J. Perera, and T. HT. Chan, "Development of a vibration based method to update axial shortening of vertical load bearing elements in reinforced concrete buildings," Engineering Structures, vol. 46, pp. 49–61, 2013.

[4] A. K. Pandey, M. Biswas, and M. M. Samman, "Damage detection from changes in curvature mode shapes," Journal of Sound and Vibration, vol. 145, no. 2, pp. 321–332, 1991.

[5] K. Roy, "Structural damage identification using mode shape slope and curvature," ASCE Journal of Engineering Mechanics, vol. 143, no. 9, pp. 04017110-1–12, 2017.

[6] J. M. Ndambi, J. Vantomme, and K. Harri, "Damage assessment in reinforced concrete beams using eigenfrequencies and mode shape derivatives," Engineering Structures, vol. 24, no. 4, pp. 501–515, 2002.

[7] N. Baghiee, M. R. Esfahani, and K. Moslem, "Studies on damage and FRP strengthening of reinforced concrete beams by vibration monitoring," Engineering Structures, vol. 31, no. 4, pp. 875–893, 2009.

[8] P. J. Cornwell, S. W. Doebling, and C. R. Farrar, "Application of the strain energy damage detection method to plate-like structures," Journal of Sound and Vibration, vol. 224, no. 2, pp. 359–374, 1999.

[9] N. Lieven and D. Ewins, "Spatial correlation of mode shapes: the coordinate modal assurance criterion (COMAC)," Proc. of the 6th International Modal Analysis Conference, Orlando, FL, 1988.

[10] Z. G. Sun, J. M. Ko, and Y-Q. Ni, "Modal indices for identifying damage location in cable-stayed Kap Shui Mun Bridge," Proc. SPIE 4337: Health Monitoring and Management of Civil Infrastructure Systems, 2001.

[11] M. Chandrashekhar and R. Ganguli, "Damage assessment of structures with uncertainty by using mode-shape curvatures and fuzzy logic," Journal of Sound and Vibration, vol. 326, no. 3, pp. 939–957, 2009.

[12] Zeng, "Index combination for structural damage detection using genetic algorithm," Dissertation, University of Mississippi, August 2020.

[13] S. B. Worley and E. K. Ervin, "Health study of reinforced concrete test bridge with pier damage," ACI Structure Journal, vol. 114, no. 4, pp. 959–967, 2017.